Priority Report

Cancer Research

Metabolic Imaging of the Human Brain with Hyperpolarized ^{13}C Pyruvate Demonstrates ^{13}C Lactate Production in Brain Tumor Patients

Vesselin Z. Miloushev[1,2,3], Kristin L. Granlund[1,2], Rostislav Boltyanskiy[1,2], Serge K. Lyashchenko[4], Lisa M. DeAngelis[3,5,6], Ingo K. Mellinghoff[3,5,6], Cameron W. Brennan[3,6,7], Vivian Tabar[3,6,7], T. Jonathan Yang[3,8], Andrei I. Holodny[1,3,6], Ramon E. Sosa[1], YanWei W. Guo[1], Albert P. Chen[9], James Tropp[10], Fraser Robb[11], and Kayvan R. Keshari[1,2,3,6]

Abstract

Hyperpolarized (HP) MRI using [1-13C] pyruvate is a novel method that can characterize energy metabolism in the human brain and brain tumors. Here, we present the first dynamically acquired human brain HP 13C metabolic spectra and spatial metabolite maps in cases of both untreated and recurrent tumors. *In vivo* production of HP lactate from HP pyruvate by tumors was indicative of altered cancer metabolism, whereas production of HP lactate in the entire brain was likely due to baseline metabolism. We correlated our results with standard clinical brain MRI, MRI DCE perfusion, and in one case FDG PET/CT. Our results suggest that HP 13C pyruvate-to-lactate conversion may be a viable metabolic biomarker for assessing tumor response.

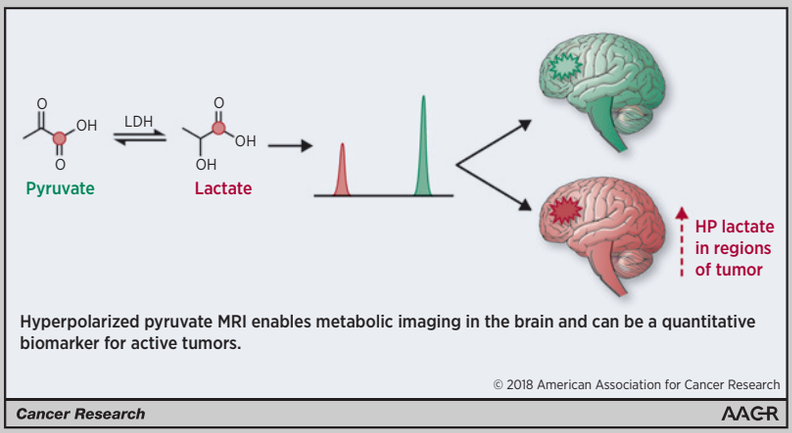

Hyperpolarized pyruvate MRI enables metabolic imaging in the brain and can be a quantitative biomarker for active tumors.

Significance: Hyperpolarized pyruvate MRI enables metabolic imaging in the brain and can be a quantitative biomarker for active tumors.

Graphical Abstract: http://cancerres.aacrjournals.org/content/canres/78/14/3755/F1.large.jpg. *Cancer Res; 78(14); 3755–60. ©2018 AACR.*

Introduction

Current "open-problems" in neuro-oncological imaging include quantifying tumor response during and following treatment on a clinically relevant timescale, differentiating recurrent/residual tumor and treatment-related changes with high specificity, classifying tumor pathological aberrations on a molecular level, and predicting the response of tumor to treatment. Metabolic biomarkers can potentially address these issues and in principle detect response or recurrence before genetic alterations or more delayed morphological changes, currently a clinical need which is unmet by conventional imaging (1). Specifically, in high-grade glioma patients, treatment-related changes (pseudo-progression) are well known to confound assessment for tumor recurrence by standard MRI (2). Multifaceted tumor changes may masquerade as apparent improvement (pseudo-response) without a survival benefit (3). Furthermore, low-grade glial tumors are currently monitored by serial imaging, potentially delaying intervention. At times, several methods for monitoring gliomas are often integrated for clinical problem solving, including MRI perfusion, ^{1}H MR spectroscopy, and occasionally ^{18}FDG PET and other emerging tracers in the research setting (4–6).

[1]Radiology, Memorial Sloan Kettering Cancer Center, New York, New York. [2]Molecular Pharmacology Program, Memorial Sloan Kettering Cancer Center, New York, New York. [3]Brain Tumor Center, Memorial Sloan Kettering Cancer Center, New York, New York. [4]Radiochemistry and Molecular Imaging Probes (RIMP) Core, Memorial Sloan Kettering Cancer Center, New York, New York. [5]Department of Neurology, Memorial Sloan Kettering Cancer Center, New York, New York. [6]Weill Cornell Medical College, New York, New York. [7]Department of Neurosurgery, Memorial Sloan Kettering Cancer Center, New York, New York. [8]Department of Radiation Oncology, Memorial Sloan Kettering Cancer Center, New York, New York. [9]GE Healthcare, Toronto, Ontario, Canada. [10]GE Healthcare, Fremont, California. [11]GE Healthcare, Aurora, Ohio.

Note: Supplementary data for this article are available at Cancer Research Online (http://cancerres.aacrjournals.org/).

V.Z. Miloushev and K.L. Granlund contributed equally to the article.

Current address for J. Tropp: Berkshire Magnetics LLC, Berkeley, CA.

Corresponding Author: Kayvan R. Keshari, Memorial Sloan Kettering Cancer Center, 1275 York Avenue, New York, NY 10065. Phone: 646-888-3631. Fax: 646-422-0247; E-mail: rahimikk@mskcc.org

doi: 10.1158/0008-5472.CAN-18-0221

Hyperpolarized (HP) MRI is a novel technology that significantly amplifies signal to noise (~10,000-fold) and can potentially address clinical needs from a unique metabolic perspective (7). HP MRI can be used to image metabolism in the human body by administering HP metabolic precursor molecules. In the current work, hyperpolarization is accomplished using the dissolution dynamic nuclear polarization method (8). Endogenously occurring molecules are hyperpolarized *ex vivo* and injected intravenously, allowing the HP label to be followed as the molecule is distributed and metabolized in the human body (9, 10).

Pyruvate is one such endogenously occurring alpha-keto acid, predominantly generated from glucose that has a central role in energy metabolism, and is suited to gauge altered cancer metabolism (11, 12). Prior (non-polarized) experiments have demonstrated that exogenous pyruvate enters the brain, and at low concentrations is metabolized similarly to glucose (13). When isotopically enriched at the first position, [1-^{13}C] pyruvate, the primary detectable metabolic products (alanine, bicarbonate, lactate, and the pyruvate hydrate) have different chemical shifts and can be differentiated using MR spectroscopic imaging (MRSI). The contributions of reductive (lactate) versus oxidative (bicarbonate) metabolism can be quantified, allowing for metabolic profiling of physiological and pathological states. Importantly, metabolite quantification in HP experiments can be performed in near real-time. Alternatively, non-polarized ^{1}H MR spectroscopy detects the steady state lactate pool when it is at high concentrations.

The pursuit of HP pyruvate as a metabolic biomarker in neuro-oncological imaging is motivated by multiple studies using preclinical rodent brain tumor models demonstrating the increased metabolic flux of HP pyruvate to lactate in tumors relative to the anesthetized rodent brain (14). Moreover, in preclinical models, decreased metabolism of HP pyruvate to lactate correlates with early treatment response following chemotherapy, suggesting that HP pyruvate may be a useful early metabolic biomarker for treatment response in human brain tumors (15, 16).

The present work illustrates the application of HP MRI to image human brain metabolism. We demonstrate the feasibility of using this approach to quantitatively interrogate dynamic metabolism in the human brain as a precedent to establishing HP pyruvate as a quantitative metabolic biomarker. We report the initial application of the technique to cases of untreated or recurrent brain tumors, providing support for further exploration into the human brain using HP MRI.

Patients and Methods

Patient recruitment

Patients were recruited under an institutional review board (IRB 14-205, PI: Keshari) approved protocol at Memorial Sloan Kettering Cancer Center (MSKCC). An investigational drug acknowledgement was granted for HP [1-^{13}C] pyruvate (IND #11259470, PI: Keshari). Written informed consent was documented for all patients. The study was performed in accordance with the Declaration of Helsinki, Belmont Report, U.S. Common Rule guidelines, and the International Ethical Guidelines for Biomedical Research Involving Human Subjects. All information was accessed, stored, and published in keeping with HIPAA protections. This report includes data from 4 patients, and 5 individual injections (one patient underwent two successful injections one hour apart). Diagnoses were: Patient 1, anaplastic oligodendroglioma; Patient 2, recurrent glioblastoma; Patient 3, metastatic melanoma; Patient 4, metastatic ovarian carcinoma. Details are provided in Supplementary Table S1.

Hyperpolarization

Dynamic nuclear polarization was performed with a 5.0 T SpinLab Hyperpolarizer (GE). The dose used (0.43 mL/kg of 250 mmol/L pyruvate) was determined in the initial clinical trial (17). The sterile fluid paths, containing [1-^{13}C] pyruvic acid (14.2 mol/L), trityl-OXO63 radical (15 mmol/L), sterile water for injection (USP), and a neutralizing base solution, were prepared under cGMP conditions at MSK Radiochemistry and Molecular Imaging Probes Core Facility and then loaded into the polarizer. Polarization times of approximately 2 to 3 hours were sufficient to attain 20% to 40% polarization. Before injection, the final injectable product conformance to the acceptance criteria, including pyruvate concentration, pH, residual EPA (electroparamagnetic agent) concentration, temperature, and polarization level, was established using the in-line automated quality control module (Supplementary Table S2). The HP sample and 20 mL saline flush were injected intravenously at a rate of 5 mL/second.

Data acquisition

Hardware. All patients were scanned on a single 3.0 T MRI (Discovery 750WB, GE Healthcare). An 8-channel ^{1}H transmit/receive head coil was used for clinical brain MRI. The multinuclear spectroscopic package (MNS) was used for ^{13}C applications. An external large field of view ^{13}C clam-shell coil (GE) was used for RF transmission. Two 4-channel ^{13}C surface coils arrays (GE) were used for signal reception. The ^{1}H body coil was used for anatomic imaging.

Sequences. Clinical brain ^{1}H MRI sequences included T_1-weighted, T_2-weighted, T_2/FLAIR, DWI, SWI, and post-contrast T_1-weighted images. T_1-weighted dynamic contrast–enhanced perfusion images (DCE) were post-processed using NordicICE (NordicNeuroLab) to generate kinetic transfer and volume constants. A fly-back echo-planar spectroscopic sequence (EPSI) was used for dynamic single axially selective slice MRSI. The field of view included the entire head (16–20 cm) with minimal aliasing in the anterior–posterior (AP) dimension, and 1.5- to 2-cm slice thickness, centered on the lesion of interest. The EPSI data were acquired Left–Right (LR) as an echo with 16 spatial points, 58 spectral points, a fly-back efficiency of 59%, initial spectral delay was approximately 25 ms, a 153 ms acquisition time, and a spectral width of 579 Hz (~18 ppm). The indirect (phase-encode) dimension was acquired AP sequentially as an echo with 16 spatial points. The temporal resolution was 4.3 seconds. A constant flip angle (10–20 degrees) was used for each time point. The dynamic sequence train was started immediately after completion of the injection flush. The dissolution, injection and subsequent dynamic imaging is completed in about 2 minutes.

Data processing

All data processing was performed in MATLAB (Mathworks Inc.) using in-house scripts, accomplishing data re-ordering, apodization, zero-filling, spatial phasing, baseline correction, and

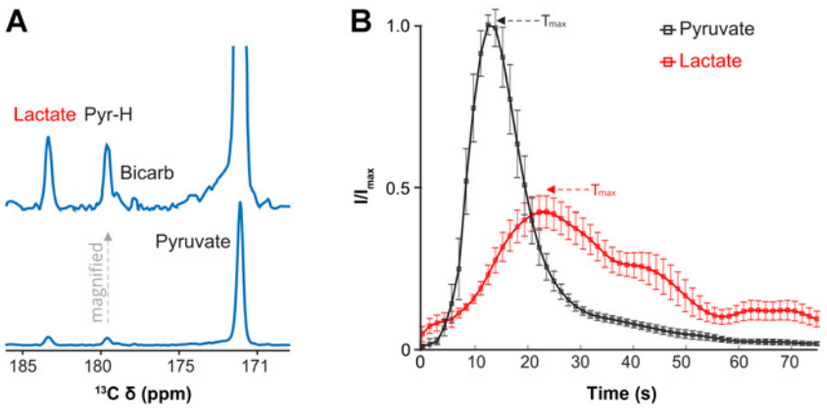

Figure 1.

First-in-human brain HP pyruvate to lactate metabolism. **A,** Mean spectrum, weighted in time, summed over the entire brain slice with accompanying scaled increased spectrum, for the first patient (Patient 1) imaged with HP pyruvate, demonstrating metabolic conversion to lactate, the pyruvate hydrate (PyrH), and putative bicarbonate (Bicarb). The top spectrum is a magnified version. **B,** Average dynamics of HP pyruvate delivery (green curve) and lactate (red curve, scaled $\times 5$) buildup over the entire brain slice (tumor and normal brain) in four patients (five injections). The mean time to maximum (T_{max}) of pyruvate (11.7 ± 1.9 s) and lactate (23.0 ± 1.3 s) signals are indicated by arrows. The relative delay in the lactate T_{max} is consistent with metabolic conversion. Curves are interpolated 3-fold for smoothing. Actual time resolution is 4.3 s. Error bars, SEM, without scaling for lactate. Vertical scale is in arbitrary units.

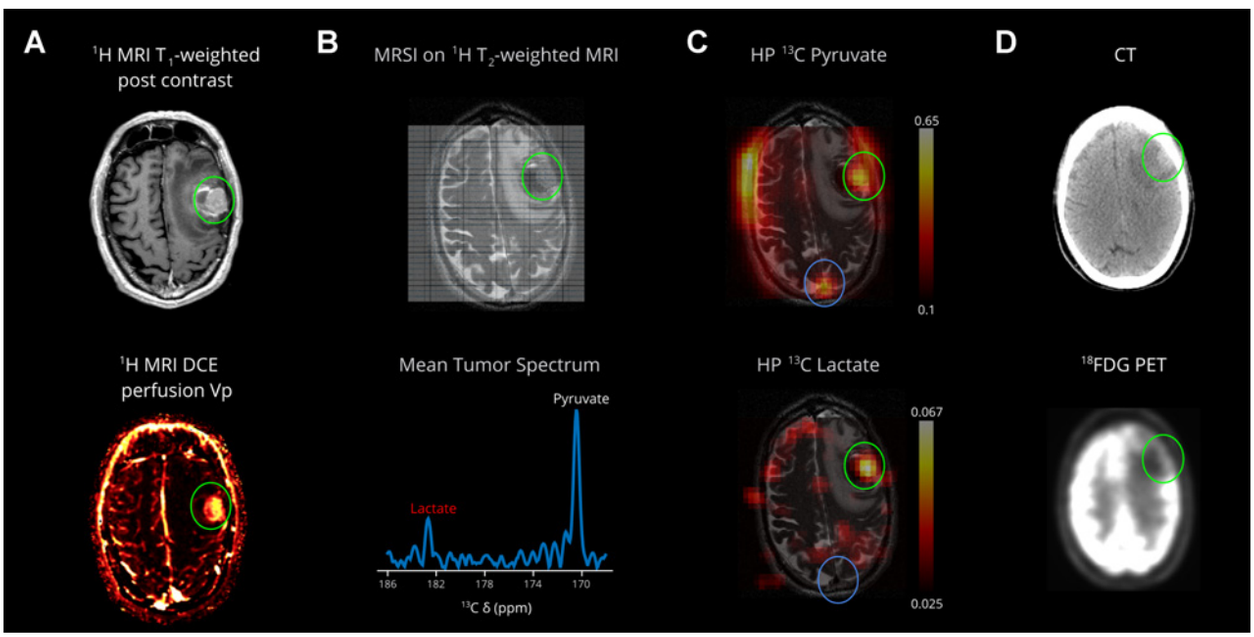

Figure 2.

First-in-human HP pyruvate imaging of a metastasis (Patient 3). **A,** The left middle frontal gyrus melanoma metastasis (green circle) has solid components laterally and hemorrhagic components medially. MRI DCE perfusion demonstrates correlate elevated plasma volume. **B,** The ^{13}C MRSI imaging grid is superimposed on a base T_2-weighted ^1H image, showing the left middle frontal gyrus hemorrhagic metastasis (green circle), left frontal mass effect and edema. The interpolated grid corresponds to a native 1-cm in-plane resolution over a 16-cm field-of-view and 2.0-cm slice thickness. Mean tumor spectrum shows pyruvate and its metabolic product lactate. **C,** The HP pyruvate map shows high signal corresponding to the metastasis, likely due to perfusion. The volume normalized pyruvate signal in the lesion is 2.8-fold higher than the entire brain. The HP lactate map shows significantly high intensity corresponding to the solid component of the metastasis, absent from the medial perilesional hemorrhagic component (**B,** T_2-weighted image, dark signal, medially). The volume normalized lactate signal in the lesion is 6.7-fold higher than the entire brain. Importantly, lactate signal in the superior sagittal sinus is low, consistent with the detected lactate being made locally in the brain, not due to delivery from outside the brain. **D,** FDG PET/CT obtained 31 days prior; the mass increased slightly between the PET/CT ($\sim 2.1 \times 1.3$ cm) and the brain MR ($\sim 2.5 \times 1.8$ cm); the brain MR also demonstrates increased hemorrhage medial to the mass and increased left frontal edema. The mass is relatively hypometabolic compared with the high cortical metabolism, which is expected to be predominantly oxidative, relative to the tumor. Lactate scale is relative to pyruvate.

coil-summation. A two-compartment model was simulated for the time evolution of dynamics to fit the composite forward kinetic rate constant for pyruvate to lactate conversion (see Supplementary Data for derivation and additional assumptions). Mean spectra and metabolite maps are absolute-value weighted averages over time and, respectively, spatial dimensions or mean spectral integrals (1 ppm). Metabolite maps are de-noised using a spatial Wiener filter and Gaussian smoothing. Volume normalized signal intensity ratios (reported as fold increases) are spectral integrals (1 ppm) from an ROI of the lesion over the entire brain slice. Figures were prepared with MATLAB and GravitDesigner (Gravit GmbH).

Results

Initial findings

First-in-human brain metabolism of HP pyruvate to lactate was readily detected, Fig. 1A. Conversion to lactate was observed over the entire brain at low-intermediate levels. Conversion to bicarbonate, was sub-optimally detected in part due to signal-to-noise limitations and technical limitations; the resonance (expected 160.9 ppm) was aliased (178.9 ppm) near the pyruvate hydrate, which was a stronger signal.

Pyruvate and lactate dynamics

The shapes of the dynamic time-courses of pyruvate delivery and lactate buildup are relatively uniform across 4 individual patients, Fig. 1B; Supplementary Table S1. The pyruvate maximum occurred at 11.7 ± 1.9 seconds and the lactate maximum occurred at 23.0 ± 1.3 seconds. These averages include the entire brain slice, including the underlying lesions, which in one patient dominated the pyruvate and lactate signals. One patient received 2 HP pyruvate injections, 1 hour apart, but concordance was not easily assessed given relatively lower polarization and SNR in the second injection.

The shape of the dynamic pyruvate signal time-course indicates that it is dominated by vascular perfusion. The shape of the dynamic lactate signal time-course is consistent with production of lactate in the brain, rather than vascular perfusion. Lactate signal was not detected in the venous compartment (superior sagittal sinus), arguing for fast essentially unidirectional flux on the time-course of the experiment (see spatial metabolite maps). The dynamic time-courses of pyruvate and lactate signals could be fit to obtain a composite forward kinetic rate k_{PL}, under significant assumptions. The values obtained in this manner are the order of 0.1 s^{-1}(mean = 0.12 s^{-1}, range = 0.08–0.16 s^{-1}, $n = 4$, Supplementary Figs. S1–S2, Supplementary Table S3).

Spatial metabolite localization

Two-dimensional spatial metabolite maps of pyruvate and lactate were constructed from spectral integrals as signal weighted sums over time. For 3 of 4 patients, spatially localized pyruvate perfusion and lactate production in the entire brain is clearly non-uniform, and appears significantly higher in cortical/juxtacortical regions rather than white matter tracts; for example, in the centrum semiovale or periventricular white matter. For one patient (Patient 3), the pyruvate and lactate signals were dominated by the lesion and vascular compartment, a feature attributed to low SNR, and significantly higher perfusion/metabolism by the lesion compared with the entire brain.

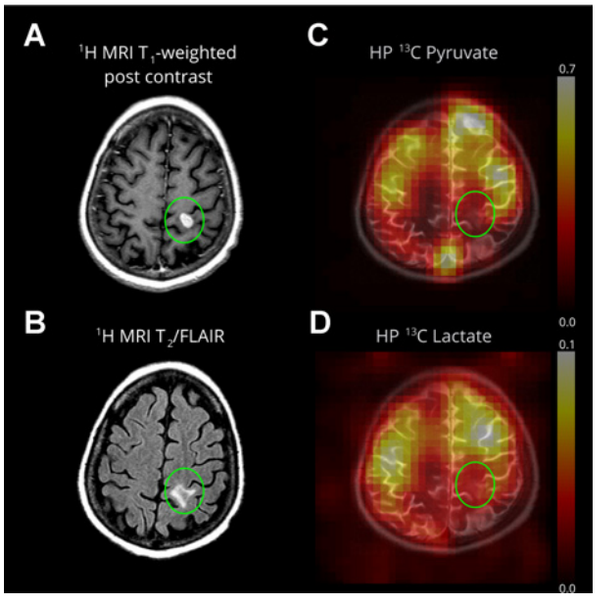

Figure 3.
Pyruvate metabolism in a small ovarian cancer metastasis (Patient 4) after systemic chemotherapy. **A,** An enhancing metastasis is located in the left postcentral gyrus (green oval). **B,** The T_2/FLAIR image demonstrates minimal surrounding edema. DCE MRI was not available for this lesion. **C,** The HP pyruvate map shows high signal corresponding to the cortex/juxtacortical regions and superior sagittal sinus. **D,** The HP lactate map similarly shows high signal in the cortex/juxtacortical regions without conspicuity in the lesion. Lactate scale is relative to pyruvate.

Brain tumors

The four patients in this study had either untreated, partly treated, or recurrent neoplasms. For example, relatively robust metabolism of HP pyruvate to lactate in an untreated melanoma metastasis (Patient 3, Fig. 2A) provides high contrast relative to background oxidative metabolism of the brain, Fig. 2B and C. Metabolism corresponds to the solid component, absent from the medial hemorrhagic component. Anecdotally, the corresponding ^{18}FDG PET/CT shows significantly higher metabolism in the non-affected cortex compared with the region of the left frontal tumor and associated edema, Fig. 2D. In contrast, a smaller ovarian cancer metastasis (Patient 4, Fig. 3A and B) did not demonstrate high pyruvate to lactate metabolism, Fig. 3C and D.

Metabolism of HP pyruvate to lactate was also detected in a lesion pathologically proven to represent treatment-related changes and recurrent glioblastoma (Patient 2), Fig. 4A and B. Pyruvate-to-lactate metabolism in this lesion is similar to the entire brain, but nevertheless the lesion is discernable on the lactate map. In contrast, a partly treated anaplastic oligodendroglioma (Patient 1) shows overall low lactate metabolism, with the apparent exception of a small region co-localized with slightly elevated perfusion, Fig. 4C and D.

Discussion

First-in-human HP pyruvate brain metabolism was detected non-invasively, dynamically and in real time, illustrated in cases of glial neoplasms and metastases. [1-^{13}C] Pyruvate was chosen due to its favorable polarization and spectroscopic properties and

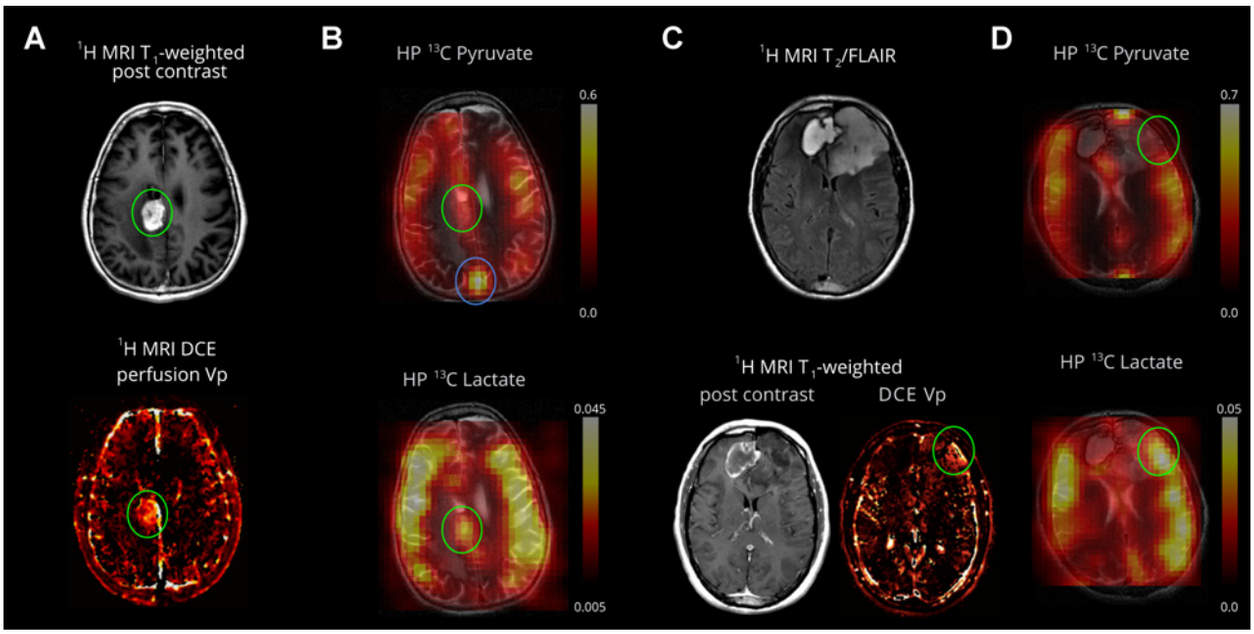

Figure 4.

Pyruvate metabolism in a recurrent glioblastoma and treatment-related changes (Patient 2, **A** and **B**) and anaplastic oligodendroglioma (Patient 1, **C** and **D**). **A,** An enhancing mass is located in the right cingulate gyrus (green oval). MRI DCE perfusion demonstrates elevated plasma volume. The resected pathological specimen demonstrated 60% viable tumor and 40% necrosis (see Supplementary Table S1). **B,** The HP pyruvate map shows high signal corresponding to the cortex/juxtacortical regions and superior sagittal sinus. The volume normalized pyruvate signal in the lesion is 1.3-fold higher than the entire brain. The HP lactate map shows mildly elevated signal corresponding to the lesion, similar to background lactate production by the brain. The volume normalized lactate signal in the lesion is 1.0-fold of the lactate over the entire brain (cortex and white matter). **C,** The T_2/FLAIR image shows an expansile left frontal mass and contracting right frontal hematoma. The left frontal mass has minimal, patchy enhancement and a small component of elevated plasma volume (green oval) visualized by DCE MRI. The resected pathological specimen demonstrated anaplastic oligodendroglioma in a background of lower-grade tumor (see Supplementary Table S1). **D,** The HP pyruvate map shows high signal corresponding to the cortex/juxtacortical regions and superior sagittal sinus, but relatively lower signal corresponding to the small hyperperfused component. The HP lactate map shows mildly elevated signal corresponding to the hyperperfused component, similar to background lactate production by the brain. **B** and **D,** Lactate scales are relative to respective pyruvate.

because pyruvate is a critical intermediate in cellular energy metabolism, with different reductive versus oxidative metabolic fates. Our imaging strategy allowed characterization of pyruvate delivery and lactate buildup as well as spatial resolution and correlation with clinical MRI methods and PET/CT.

On the basis of preclinical studies, we expected that untreated or recurrent tumor would display high lactate production. Our results are concordant, illustrated best by an untreated melanoma metastasis that demonstrated high lactate production in its solid component. The hemorrhagic component had absent signal, probably due to both susceptibility effects and absent metabolism on the time-scale of the experiment. Indeed, HP lactate production would not be expected in necrotic tumor components even if steady-state lactate is elevated by ^{1}H MRSI methods (18). A smaller ovarian cancer metastasis did not show conspicuous lactate production but this could be for a variety of reasons, including prior systemic chemotherapy and inherent tumor differences. A recurrent glioblastoma lesion composed of 60% viable tumor and 40% necrosis demonstrated lactate production similar to the background brain. We note, however, that this represents one "snap-shot" in time, and reconcile this with the unique ability of HP MRI to potentially characterize changes in the lesion over the treatment time-course. Furthermore, different tumor pathologies and differential treatment may manifest as a variety of metabolic profiles; the absence of a baseline study and an adequately powered cohort size are limitations of this small pilot study of a novel technique. Ultimately quantifying tumor heterogeneity and separating contributions from recurrent tumor and treatment-related changes may require acquisition of the time dependent lactate and bicarbonate signals and potentially other HP precursor molecules.

Furthermore, we report the first anecdotal comparison of HP MRI with ^{18}FDG PET/CT in humans. In this case, the untreated hemorrhagic metastasis demonstrated high lactate production and co-localized to a region of FDG hypometabolism, relative to unaffected cortex. This may be due to the possibility that while FDG uptake represents the fate of all glucose, HP lactate derived from pyruvate is sensitive to one side of glycolytic utilization, revealing differential metabolism. We consider the alternatives, that the lesion may be dominated by hemorrhage and adjacent edema, or too small to adequately characterize by PET/CT, to be less likely. Although many more studies are necessary to interrogate differences between metabolism assessed with ^{18}FDG PET and HP MRI, these exciting results provide a basis to pursue those studies.

Within limitations of our imaging strategy, both pyruvate perfusion and lactate production were predominantly localized to the cortical/juxtacortical regions, an observation consistent with higher cortical perfusion and vascular coupling of neuronal activation/metabolism known from other techniques. This observation naturally raises concern for limitations in assessing cortical or juxta-cortical lesions, similar to limitations in ^{18}FDG PET. In

principle, this limitation is similar to bland MRI perfusion measurements, and the amplitude and kinetics of lactate production should help to distinguish neoplasm from the normal brain as demonstrated in preclinical models.

Finally, we note two clear extensions of our work. First, we simulated pyruvate to lactate dynamics using a simplified two-compartment model. The motivation for this analysis was to quantify inherent brain metabolism with a few parameters, accounting for the technical and spectroscopic methods which modulate the acquired signal. The values obtained in this manner for k_{PL} (mean $= 0.12\ s^{-1}$, range $= 0.08–0.16\ s^{-1}$) are slightly larger than those previously reported in preclinical models (14, 19), possibly due to effects of anesthesia, interspecies differences, and modeling differences. Second, our metabolite maps of pyruvate are analogous to relative cerebral blood volume maps usually obtained from dynamic susceptibility contrast techniques, from which relative cerebral blood flow can be derived (20); we note that the metabolite maps are not leakage-corrected, probably in part reflecting the differences to the presented DCE maps. Nevertheless, the current work is also a first-in-human demonstration of brain perfusion using HP MRI.

Looking forward, pyruvate has the potential to elucidate the differential metabolism of specialized brain regions/networks, characterize functional states, and shed light on the highly coupled metabolism of neurons and astrocytes. In this preliminary study, we demonstrated metabolism of HP pyruvate in the human brain, with applications to metabolic characterization of brain tumors. Further careful imaging trials will be necessary to determine clinical utility. Notwithstanding technical limitations, and multiple avenues for improvement, this technique offers a view of brain metabolism that is relatively unprecedented.

Disclosure of Potential Conflicts of Interest

No potential conflicts of interest were disclosed.

Authors' Contributions

Conception and design: S.K. Lyashchenko, A.I. Holodny, F. Robb, K.R. Keshari
Development of methodology: K.L. Granlund, R. Boltyanskiy, S.K. Lyashchenko, A.P. Chen, J. Tropp, F. Robb, K.R. Keshari
Acquisition of data (provided animals, acquired and managed patients, provided facilities, etc.): K.L. Granlund, L.M. DeAngelis, I.K. Mellinghoff, C.W. Brennan, V. Tabar, T.J. Yang, R.E. Sosa, Y.W.W. Guo, K.R. Keshari
Analysis and interpretation of data (e.g., statistical analysis, biostatistics, computational analysis): V.Z. Miloushev, R. Boltyanskiy, I.K. Mellinghoff, A.I. Holodny, A.P. Chen, K.R. Keshari
Writing, review, and/or revision of the manuscript: V.Z. Miloushev, K.L. Granlund, S.K. Lyashchenko, L.M. DeAngelis, I.K. Mellinghoff, C.W. Brennan, A.I. Holodny, R.E. Sosa, A.P. Chen, F. Robb, K.R. Keshari
Administrative, technical, or material support (i.e., reporting or organizing data, constructing databases): L.M. DeAngelis, A.I. Holodny, R.E. Sosa, F. Robb, K.R. Keshari
Study supervision: R.E. Sosa, K.R. Keshari

Acknowledgments

We thank Kyung Peck for illuminating discussions. We acknowledge the following funding sources: NIH P30 CA008748 Cancer Center Support Grant (to V.Z. Miloushev, K.L. Granlund, R. Boltyanskiy, S.K. Lyashchenko, L.M. DeAngelis, I.K. Mellinghoff, C.W. Brennan, V. Tabar, T.J. Yang, A.I. Holodny, R.E. Sosa, Y.W. Guo, and K.R. Keshari). NIH R00 EB014328 and R01 CA195476 (to K.R. Keshari). MSKCC Radiology Development Project Grant (to V.Z Miloushev). Dana Foundation (to K.R. Keshari, V.Z. Miloushev, C.W. Brennan, A.I. Holodny, I.K. Mellinghoff, and L.M. DeAngelis). Center for Experimental Therapeutics, MSKCC (to K.R. Keshari).

Received January 31, 2018; revised March 10, 2018; accepted May 10, 2018; published first May 16, 2018.

References

1. Hu S, Balakrishnan A, Bok RA, Anderton B, Larson PEZ, Nelson SJ, et al. (13) C-pyruvate imaging reveals alterations in glycolysis that precede c-MYC induced tumor formation and regression. Cell Metab 2011;14:131–42.
2. Wen PY, Chang SM, Van den Bent MJ, Vogelbaum MA, Macdonald DR, Lee EQ. Response assessment in neuro-oncology clinical trials. J Clin Oncol 2017;35:2439–49.
3. Huang RY, Neagu MR, Reardon DA, Wen PY. Pitfalls in the neuroimaging of glioblastoma in the era of antiangiogenic and immuno/targeted therapy - detecting illusive disease, defining response. Front Neurol 2015;6:33.
4. Bulik M, Jancalek R, Vanicek J, Skoch A, Mechl M. Potential of MR spectroscopy for assessment of glioma grading. Clin Neurol Neurosurg 2013;115:146–53.
5. Venneti S, Dunphy MP, Zhang H, Pitter KL, Zanzonico P, Campos C, et al. Glutamine-based PET imaging facilitates enhanced metabolic evaluation of gliomas *in vivo*. Sci Transl Med 2015;7:274ra17.
6. Law M, Yang S, Wang H, Babb JS, Johnson G, Cha S, et al. Glioma grading: sensitivity, specificity, and predictive values of perfusion MR imaging and proton MR spectroscopic imaging compared with conventional MR imaging. Am J Neuroradiol 2003;24:1989–98.
7. Ardenkjaer-Larsen JH, Fridlund B, Gram A, Hansson G, Hansson L, Lerche MH, et al. Increase in signal-to-noise ratio of >10,000 times in liquid-state NMR. Proc Natl Acad Sci U S A 2003;100:10158–63.
8. Abragam A, Goldman M. Principles of dynamic nuclear polarisation. Rep Prog Phys 1978;41:395.
9. Golman K, Ardenkjaer-Larsen JH, Petersson JS, Mansson S, Leunbach I. Molecular imaging with endogenous substances. Proc Natl Acad Sci U S A 2003;100:10435–9.
10. Keshari KR, Wilson DM. Chemistry and biochemistry of 13C hyperpolarized magnetic resonance using dynamic nuclear polarization. Chem Soc Rev 2014;43:1627–59.
11. Warburg O. On the origin of cancer cells. Science 1956;123:309–14.
12. Ward PS, Thompson CB. Metabolic reprogramming: a cancer hallmark even warburg did not anticipate. Cancer Cell 2012;21:297–308.
13. Gonzalez SV, Nguyen NH, Rise F, Hassel B. Brain metabolism of exogenous pyruvate. J Neurochem 2005;95:284–93.
14. Park JM, Josan S, Jang T, Merchant M, Yen Y-F, Hurd RE, et al. Metabolite kinetics in C6 rat glioma model using magnetic resonance spectroscopic imaging of hyperpolarized [1–13C]pyruvate. Magnet Reson Med 2012;68:1886–93.
15. Park I, Bok R, Ozawa T, Phillips JJ, James CD, Vigneron DB, et al. Detection of early response to temozolomide treatment in brain tumors using hyperpolarized 13C MR metabolic imaging. J Magn Reson Imaging 2011;33:1284–90.
16. Chaumeil MM, Ozawa T, Park I, Scott K, James CD, Nelson SJ, et al. Hyperpolarized 13C MR spectroscopic imaging can be used to monitor Everolimus treatment *in vivo* in an orthotopic rodent model of glioblastoma. Neuroimage 2012;59:193–201.
17. Nelson SJ, Kurhanewicz J, Vigneron DB, Larson PE, Harzstark AL, Ferrone M, et al. Metabolic imaging of patients with prostate cancer using hyperpolarized [1-(1)(3)C]pyruvate. Sci Transl Med 2013;5:198ra08.
18. Maher EA, Marin-Valencia I, Bachoo RM, Mashimo T, Raisanen J, Hatanpaa KJ, et al. Metabolism of [U-(13)C]glucose in human brain tumors *in vivo*. NMR Biomed 2012;25:1234–44.
19. Park I, Larson PE, Tropp JL, Carvajal L, Reed G, Bok R, et al. Dynamic hyperpolarized carbon-13 MR metabolic imaging of nonhuman primate brain. Magn Reson Med 2014;71:19–25.
20. Petrella JR, Provenzale JM. MR perfusion imaging of the brain: techniques and applications. Am J Roentgenol 2000;175:207–19.